

Fabrication of graphene–TiO₂ nanocomposite with improved photocatalytic degradation for acid orange 7 dye under solar light irradiation

VENKATA RAMANA POSA, VISWADEVARAYALU ANNAVARAM and
ADINARAYANA REDDY SOMALA*

Department of Materials Science & Nanotechnology, Yogi Vemana University, Kadapa 516003, India

MS received 23 September 2015; accepted 4 January 2016

Abstract. In this study, photodegradation of the non-biodegradable azo dye acid orange 7 (AO7) was selected as modal target in aqueous solution using graphene–TiO₂ (GR–TiO₂) hybrid nanocomposite, was well investigated and elucidated. The crystal phase, special surface area, microscopic analysis of the GR–TiO₂ and also, chemical state of the photocatalysts were studied by powdered X-ray diffraction (PXRD), Raman spectrum, field emission scanning electron microscopy (FESEM), transmission electron microscopy (TEM), high resolution scanning electron microscopy (HRTEM), X-ray photoelectron spectroscopy (XPS), Brunauer Emmette Teller (BET) method and photoluminescence spectroscopy (PL). During photocatalysis, the GR–TiO₂ nanocomposite improved photocatalytic performance compared with that of pure TiO₂ towards AO7 organic azo-dye degradation. The reusability test of photocatalytic activity was also examined. A conceivable reaction mechanism was suggested and nattered on the basis of tentative effects. Therefore, the GR–TiO₂ nanomaterial can be widely used as a photocatalyst for treating the organic dye contaminant in the field of environmental protection.

Keywords. Hybrid material; GR–TiO₂ nanocomposite; acid orange 7 dye; photocatalytic activity; solar light.

1. Introduction

Graphene is considered to be a marvellous material and plays a vital role among all the members of the carbon group [1]. Since the invention of CNTs and C₆₀, graphene is used in the applications of electronics and in the field of materials science [2]. Graphene has many super natural properties like high electrical conductivity, greater mechanical elasticity, huge surface area, high carrier transport mobility due to atomically dense and 2D sheet composed of sp²-bonded carbon atoms ordered in a honeycomb structure [3]. When used to modify supplementary materials, graphene can retard the recombination of electron–hole pairs that are photochemical or electrochemical [5–7]. For this reason, graphene–supported semiconductor materials are considered as photocatalysts for degradation of pollutants as well as photocatalytic water splitting [8,9]. TiO₂ is a non-toxic and excellent photocatalyst material which is used for the degradation of environmental pollutants among all the semiconductors [10]. TiO₂–carbon nanocomposite material shows high photocatalytic activity compared with the bare TiO₂. However, TiO₂ has a high band gap (3.2 eV) and absorb little amount of solar light, about 5% in the ultraviolet region can be used [11]. Therefore, to enhance the activity of the solar light utilization, the progress of photocatalyst with improved efficiency

under extended range of visible light irradiation is necessary. TiO₂ very well combined with carbon-based materials to enhance photocatalytic efficiency and to overcome these type of problems [12]. Graphene–TiO₂ nanocomposite is reasonable to predict great potential and more interfacial contact, hence considered as a advantageous material to improve the photocatalytic activity of TiO₂. Water-soluble organic dye, acid orange 7, consists of azo functional group (–N=N–), acts as carcinogenic and causes severe health problems to the lives of people [13]. Photocatalysis is very cheap cost and ecofriendly method to degrade organic dyes [14–16]. From recent investigations, graphene–TiO₂ composites were successfully fabricated and applied for photocatalysis. Muthirulan *et al* [17,18] demonstrated the fabrication of titanium dioxide (TiO₂)–graphene (GR) (TiO₂–GR) nanocomposites for acid orange 7 (AO7) degradation under UV irradiation. Liang *et al* [19] communicated that a hybrid material of graphene–TiO₂ for Rh-B degradation. Hsieh *et al* [20] proposed that degradation of AO7 dye under visible light using Pt–TiO₂/graphene nanocatalysts. However, very little work has been conducted on the photocatalytic activity of GR–TiO₂ photocatalyst to acid orange 7. The purpose of this paper is fabrication and exploration of the potential of a hybrid material specifically graphene–TiO₂ for the degradation of the AO7 dye under solar light. The decomposition kinetics and mechanism of the photocatalysts were also studied.

*Author for correspondence (anreddyphd@gmail.com)

2. Experimental

2.1 Synthesis of graphene oxide

Graphene oxide was synthesized by the modified Hummers method [21]. In a typical procedure, about 5 g of graphite flakes were added to 115 ml of concentrated (98%) H_2SO_4 in an ice bath with constant stirring for 30 min. A 15 g of KMnO_4 was added slowly to the above mixture with stirring and cooling for 30 min. Further, 2.5 g of NaNO_3 was mixed with continuous stirring for 1 h, so that the temperature of the mixture was maintained below 288 K during the process. The temperature of mixture then raised to 313 K with water bath, and the mixture was stirred continuously for 30 min. Then, the mixture was diluted by 800–1000 ml of distilled water, then the temperature was raised to 371 K. Then H_2O_2 (30%) was added to the mixture until gas fruition was stopped, followed by filtering. The colour of the dispersion turned from black to yellow. The final reaction mixture was washed continuously with 1 M HCl (5%) and distilled water until the pH of the solution reached ~ 7 . Then, the washed compound was dried in vacuum oven at 333 K to obtain graphene oxide (GO). The chemical route synthesis is shown in figure 1.

2.2 Materials

Natural graphite flakes were commercially obtained from Sigma-Aldrich. In addition, titanium isopropoxide (TIP), sulphuric acid (H_2SO_4), potassium manganese oxide (KMnO_4),

sodium nitrate (NaNO_3), sodium hydroxide (NaOH), hydrogen peroxide (H_2O_2), hydrochloric acid (HCl) and acid orange 7 dye, all these chemicals procured from the Merck and used without further refinement and ethanol was supplied by China Medicine Co. Ltd. The double-distilled water was used for the total process.

2.3 Synthesis of graphene– TiO_2 nanocomposite

To synthesize graphene– TiO_2 nanocomposite, about 90 mg of as-prepared GO was spread in 60 ml of ethanol by ultrasonication for 1 h, then 1.5 ml of TIP was mixed into the suspension. The suspended mixture was stirred at room temperature for 30 min. Then, 15 ml of double-distilled water and 0.5 ml of HCl (1 M) was slowly added dropwise and the reaction mixture was stirred under N_2 atmosphere at room temperature for 24 h. The product was then centrifuged and cleaned with double-distilled water to eliminate any remaining organic residue. Then, GR– TiO_2 was dried at 353 K in a hot air oven.

2.4 Setting up of standard solution

Acid orange 7 was obtained from Merck and used without further refinement. 1000 mg l^{-1} solution was ready by dissolving suitable volume of dye in H_2O and stored in dim-coated flask and diluted by adding required quantity of double-distilled H_2O to the standard dye solution (according to necessity).

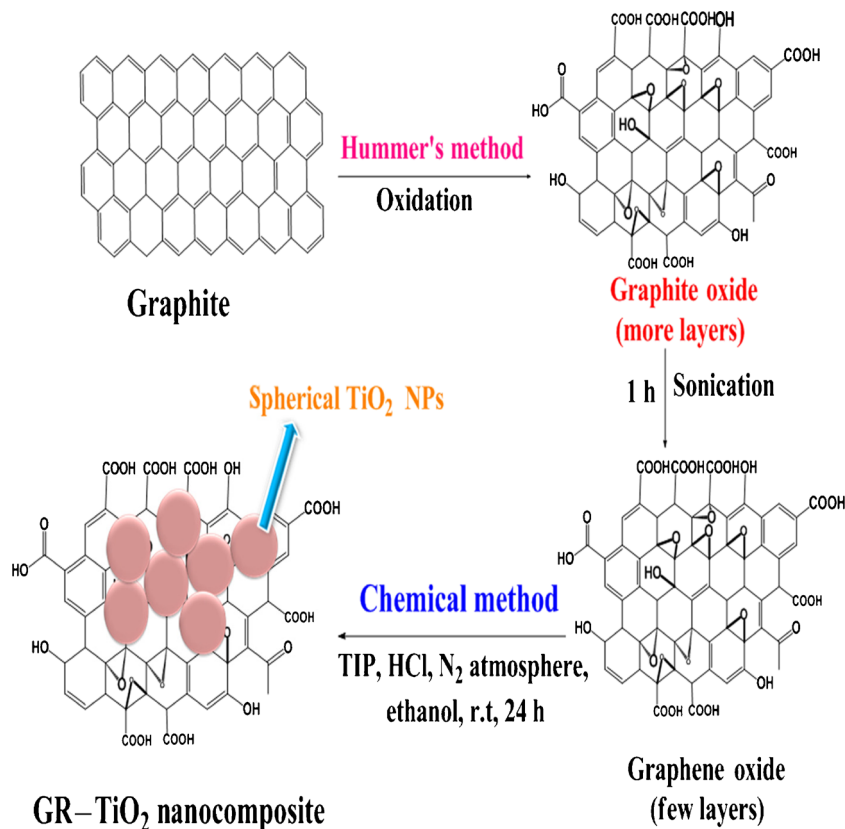


Figure 1. Chemical route synthesis of GR– TiO_2 nanocomposite.

2.5 Characterization

The resulting materials were characterized by various techniques including powder X-ray diffractometry (PXRD)

Bruker D8 using CuK α 1 (1.5406 Å) and K α 2 (1.54439 Å) radiations, Raman spectra were recorded using a WiTec alpha 200 SNOM system. Microanalysis of as-obtained materials were studied by a field emission scanning electron

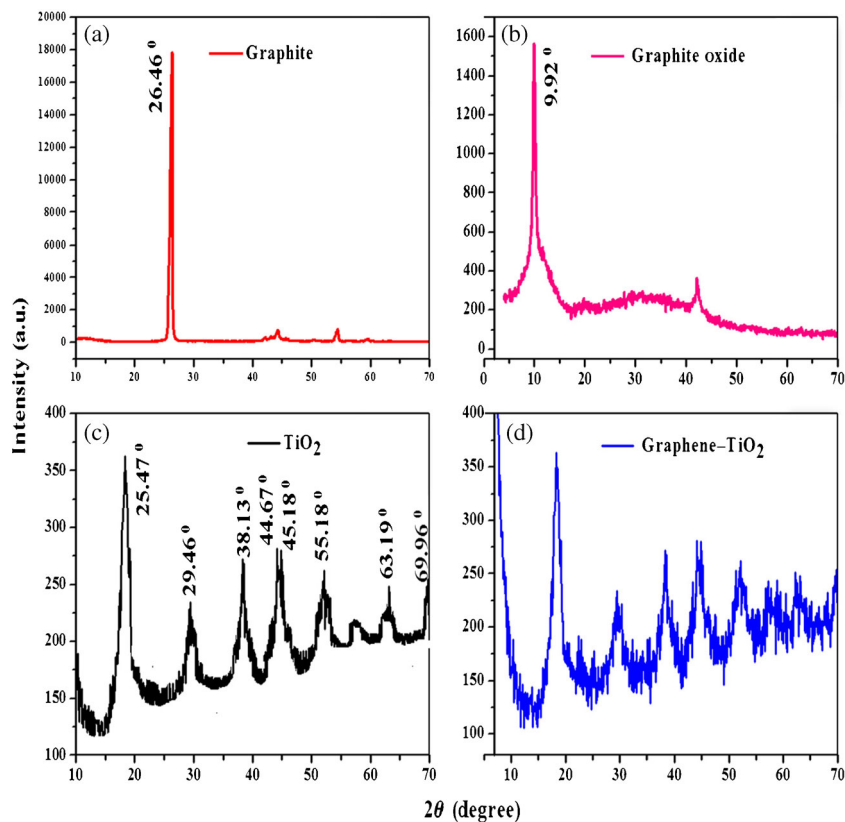


Figure 2. P-XRD patterns of (a) graphite, (b) graphite oxide, (c) TiO₂ and (d) graphene-TiO₂.

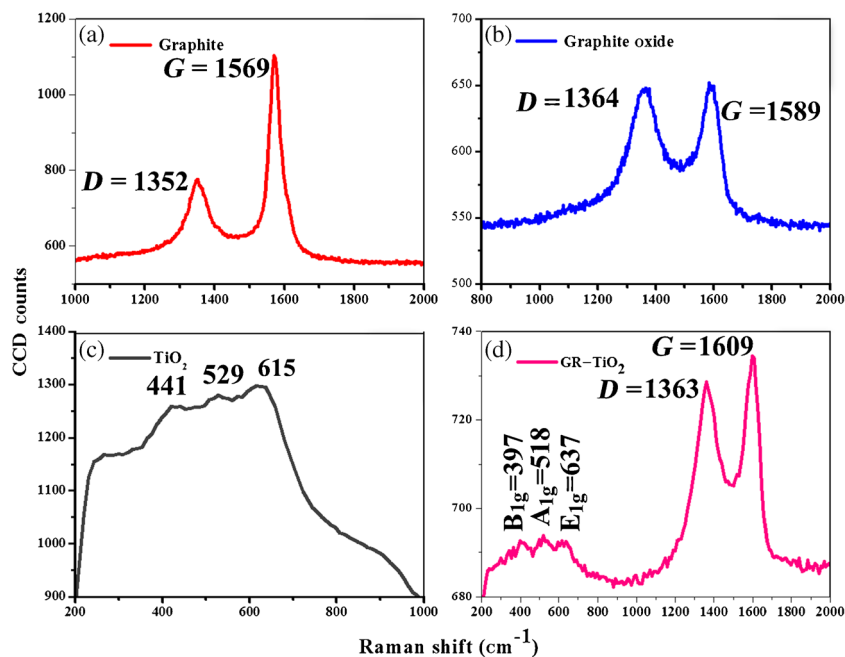


Figure 3. Raman spectrum of (a) graphite, (b) graphite oxide, (c) TiO₂ and (d) GR-TiO₂.

microscope (FESEM) imaging with energy dispersive spectroscopy (EDS) using a Carl Zeiss Supra 55 operating at 5 and 20 kV, structure analyses were conducted by a transmission electron microscope (TEM) and measurements were performed on a JEOL 3010 at 200 kV, ultraviolet–visible absorption spectra were recorded using Shimadzu-1800. X-ray photoelectron spectra (XPS) were noted down on a KRATOS AXIC 165 equipped with MgK α radiation. All binding energies were referenced to C 1s at 284.8 eV. N₂ adsorption and desorption tests were conducted on Micrometrics ASAP 2020. The samples were outgassed at 150°C for 12 h in a dynamic vacuum before physisorption measurements. The specific surface area was calculated using Brunauer Emmette Teller (BET) method. A photoluminescence spectrum (PL) was recorded by using JOBIN YVON Fluorolog-3 spectrofluorometer with a YSOW Xenon lamp used as broad band source. The absorption of residual AO7 was resolved by visible spectrophotometer (Shimadzu-1800 UV–visible spectrometer) based on the absorbance at 483 nm wavelength. The pH of the solution was calculated by using digital Elico pH meter. Solar light intensity was checked by TES 1332A Lux meter.

2.6 Photocatalytic efficiency tests

Photocatalytic efficiency of the photocatalysts was esteemed by photodegradation of AO7 under solar light irradiation at 11.00 am and 1.00 pm in the summer season at Yogi Vemana University, Kadapa, Andhra Pradesh, India. The intensity of the solar light is found to be around one lakh flux. Organic dye solutions (30 ml, 20 mg l⁻¹) containing 30 mg of catalysts were put in a closed round bottom flask. To ensure good absorption–desorption equilibrium, first sonicated for 5 min,

and then stirred in dark condition for 30 min. For every regular time intervals, 3 ml of samples were taken in the presence of solar light irradiation. It is centrifuged and separated. This is recorded as base concentration C_{on} . The absorption band maximum of supernatants in the AO7 dye was investigated by recording variations using a Shimadzu-1800 UV–visible spectrometer to calculate the optical absorption at 483 nm. This is denoted as C_t . In the photocatalytic efficiency tests, the degree of degradation of the dye; in terms of the values of percentage degradation has been designed using the following correlation:

$$\text{Photodegradation \%} = 100 * (C_{on} - C_t) / C_t.$$

Here, C_{on} is the initial concentration of the dye before solar light irradiation and C_t is the final concentration of the dye at given time [17,18].

3. Results and discussion

3.1 XRD patterns

The crystallographic structure of the GR–TiO₂ nanocomposite, TiO₂, graphite oxide and graphite was evidenced by XRD measurements. Figure 2a exhibits intense crystalline peak at 26.46°. This i denoted as graphite. After oxidation, the peak shifts to 9.92°, which corresponds to graphite oxides. It is found from figure 2d that the peaks at 2θ values of 25.47, 29.46, 38.13, 44.67, 45.18, 63.19 and 69.96° which can be indexed to (101), (004), (200), (105), (211), (204) and (116) from the graphene–TiO₂ which was relatively the same as that from anatase TiO₂ crystal planes (figure 2c) (JCPDS file

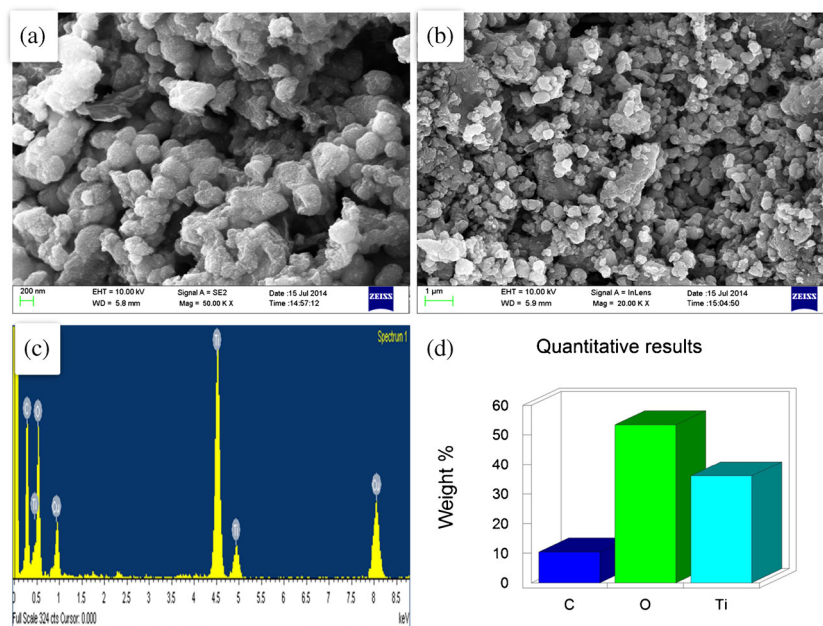


Figure 4. (a, b) FE-SEM images of GR–TiO₂ nanocomposite, (c) EDAX spectrum of GR–TiO₂ composite and (d) element weight % of as-prepared GR–TiO₂.

no: 89-4921) [22]. Due to the low amount of graphene, there is no characteristic diffraction peak observed at XRD pattern.

3.2 Raman spectroscopy analysis

The presence of both carbon and TiO₂ can be confirmed from the Raman spectra. Figure 3 shows the Raman spectra of graphite, graphite oxide, TiO₂ and GR-TiO₂ nanocomposites. From figure 3d, Raman spectra clearly seen as vibration peaks at 397 (B_{1g}), 518 (A_{1g}) and 637 cm⁻¹ (E_{1g}) which are characteristics of anatase TiO₂ [23]. The D band represents the sp³ defects in carbon, and the G band is plane vibrations of sp² bonded carbons. The D and G bands intensity ratio typically reveals the order of defects in graphene [24]. Raman spectrum of GR-TiO₂ showed the presence of D and G bands at 1364 and 1589 cm⁻¹, respectively (figure 3d). In comparison to GO ($I_D/I_G = 0.99$) and GR-TiO₂ ($I_D/I_G = 1.02$), the increased I_D/I_G peak intensity ratio is in the GR-TiO₂. This demonstrates the strong interaction between graphene and TiO₂.

3.3 Morphology and EDS study

Figure 4 shows the FESEM images of as-prepared GR-TiO₂ which possesses sphere morphology. Energy dispersive spectroscopy (EDS) proved the presence of carbon and TiO₂ in

those materials and is shown in figure 4c. These spectra indicate TiO₂ with high purity which have been successfully synthesized in this study. The C element should mainly originate from graphene. The oxygen and Ti element mainly come from the TiO₂. Figure 4d shows Ti element of strong K_α at 4.51 KeV and K_β peak at 4.92 keV, while a moderate K_α peak of the O element at 0.52 keV and also listed about the samples elemental microanalyses (wt%). Figure 5 shows the GR-TiO₂ catalyst TEM images and it can be observed that spherically polycrystalline TiO₂ nanoparticles with average facet of 3–6 nm are supported on the translucent graphene (figure 5a and b). Hence, in this structure, the graphene acts as a platform for TiO₂ components. Figure 5b shows the SAED pattern of the graphene-TiO₂ material, in this, lattice spacing of TiO₂ is 3.5 Å. As shown in figure 5c and d, HRTEM images evidently illustrate the crystalline nature of the GR-TiO₂ nanocomposite.

3.4 XPS exploration

XPS was analysed to the surface chemical formation of the hybrid materials. The XPS survey spectrum of graphene-TiO₂ clearly presents the photoelectron peaks of Ti, O and C, confirming the existence of GR in the sample (figure 6a) in graphene-TiO₂. From the panel b, it can be observed that 285 eV, which may be assigned to the elemental carbon, carbonates and Ti-O-C bond. The corresponding XPS

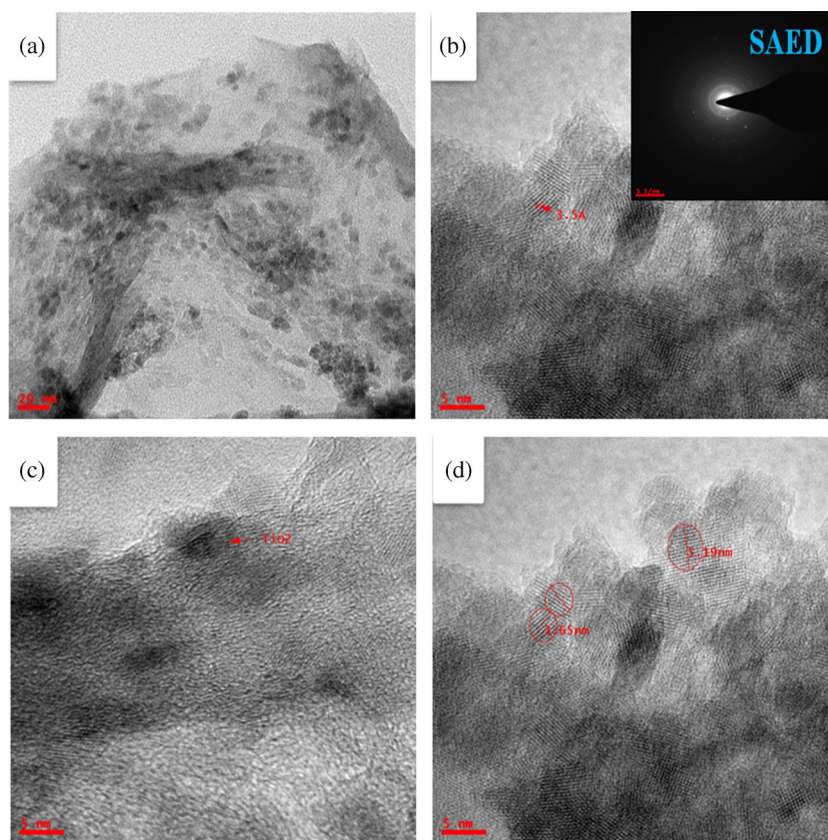


Figure 5. (a, b) TEM images (inside SAED pattern) and (c, d) HRTEM images of GR-TiO₂ nanohybrid material.

spectrum of the two well-determined peaks at 461 and 467 eV were observed from the Ti 2p core-level spectrum (figure 6b), which can be assigned to Ti 2p 1/2 and Ti 2p 3/2 spin

orbital components in TiO₂, respectively. For the O 1s electrons (as shown in figure 6d), sample exhibits a strong peak at around 533.5 eV corresponding to the Ti–O bond [24].

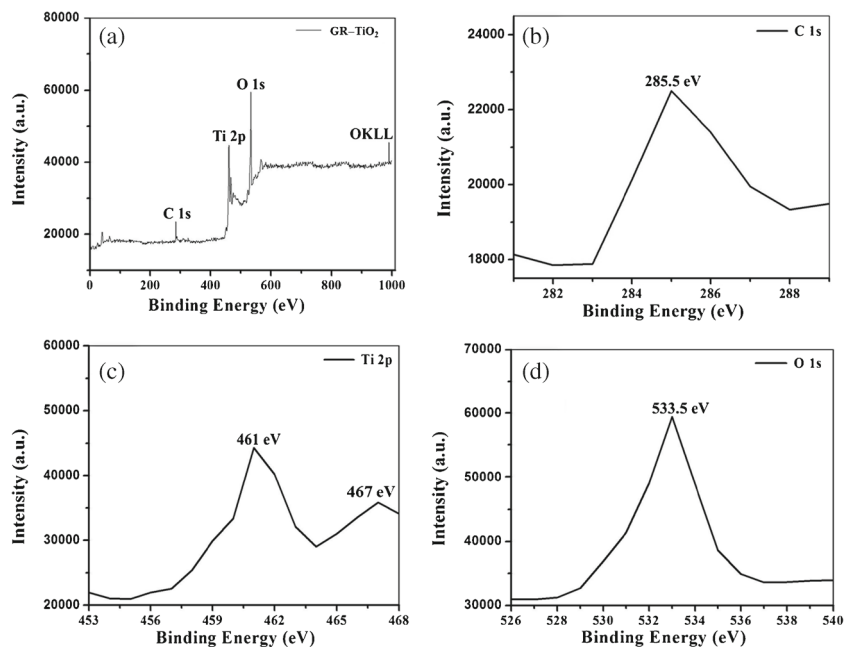


Figure 6. (a) XPS survey spectrum of GR–TiO₂ and high-resolution scans of the binding energies of (b) C 1s, (c) Ti 2p and (d) O 1s electrons in the composites.

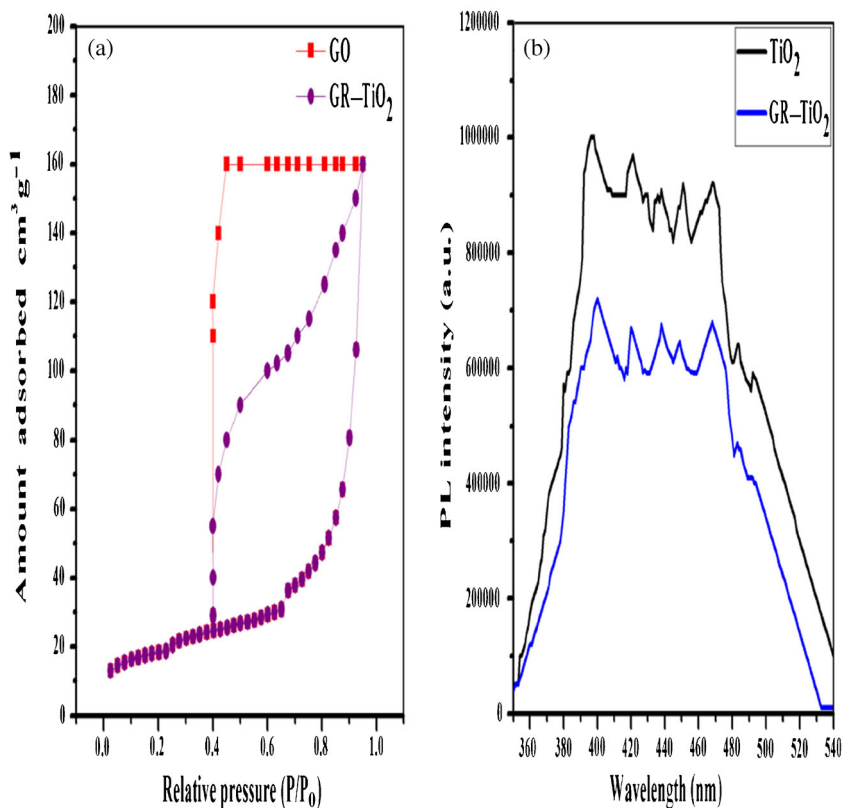


Figure 7. A typical nitrogen adsorption–desorption isotherms of GO and 0.3% GR–TiO₂ and PL spectra of as-prepared TiO₂ and 0.3% GR–TiO₂ materials.

3.5 BET and PL spectra study

The specific surface area of the prepared graphene-TiO₂ nanocomposites calculated by the multipoint BET method. Surface area of GR-TiO₂ (162.3 m² g⁻¹) was lower than that of GO (186 m² g⁻¹) due to the high density and low surface area of TiO₂ polycrystalline nanoparticles (figure 7a). PL emission spectrum is useful to disclose the efficiency of charge carrier catching, immigration and distribution. The excitation wavelength of catalyst is 320 nm. In the literature, it was reported that PL of TiO₂ and 0.3% GR-TiO₂ composite were in the range of 350–550 nm and the electron-hole recombination rate was lower for GR-TiO₂-based composites (figure 7b).

3.6 Photocatalytic activities and photodegradation mechanism

Figure 8a shows photocatalytic skills of altered samples irradiated with solar light. The adsorption of these solutions decreased gradually with irradiation time. The characteristic adsorption of AO7 almost disappeared after 60 min, and the

dye of AO7 solution changed gradually from golden yellow to colourless. The GR-TiO₂ shows the degradation of AO7 removal is 99%, TiO₂ removal is 47%, GR removal is 20% and mechanical mixing of GR + TiO₂ is 66%, suggesting that GR-TiO₂ is active catalyst. Figure 8b shows the absorption curves progressively with rising exposure time from 0 to 60 min. Figure 8c shows the optimum value of GR-TiO₂ catalyst (0.3% GR) exhibited even better photocatalytic performance than that of P25 under solar light. Pure TiO₂ rate constant, $k = 0.065 \text{ min}^{-1}$ and 0.3% GR-TiO₂ nanocomposite rate constant, $k = 0.112 \text{ min}^{-1}$. Therefore, the degradation efficiency of GR-TiO₂ composites is slightly two times higher than that of bare TiO₂. The photocatalyst reusability was important property for effective practical applications. Three successive batch runs of the AO7 degradation reaction were conducted by using the recycled catalysts under the tested reaction conditions. The next run was carried out by recovering the catalyst from the above reaction mixture and was washed with double-distilled water and dried. The recycling test results of the most active GR-TiO₂ catalyst, represented by AO7 decolorization, are shown in figure 8d. After the third run, the AO7 removal was still about 92% at 60 min, demonstrating the satisfactory reusability

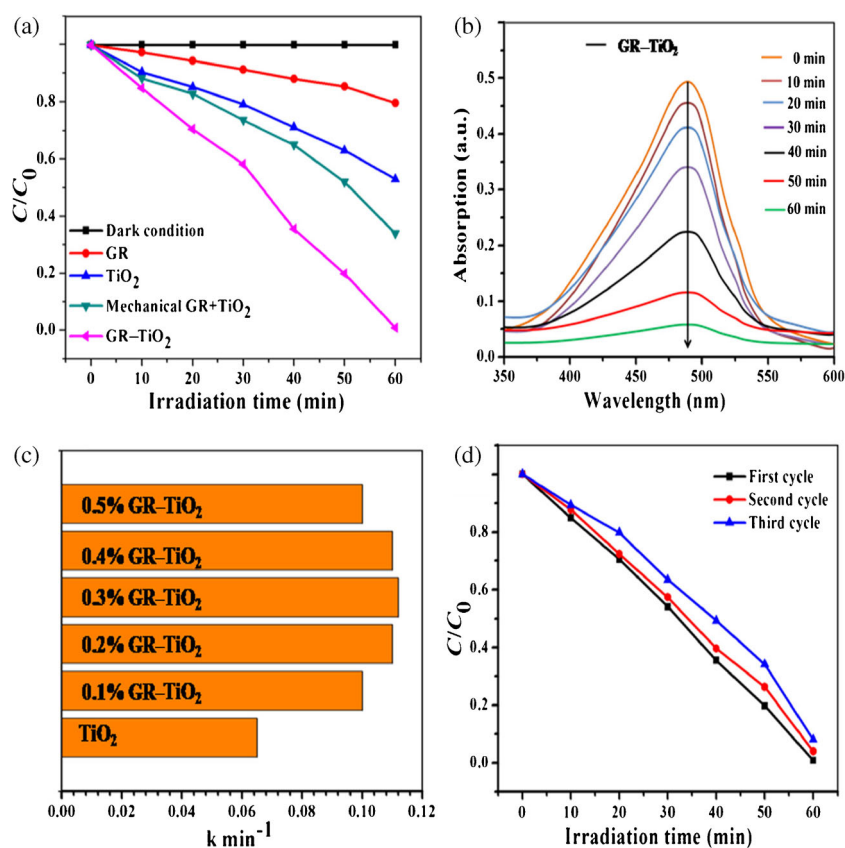


Figure 8. (a) The evaluation of degradation of AO7 at different catalysts such as GR, TiO₂, mechanical GR+TiO₂ under solar light irradiation. (b) The display of UV-Vis spectra for AO7 solution during the photocatalysis process with GR-TiO₂. (c) Photocatalytic degradation rate constant (k) of AO7 for the photocatalysts. (d) Re-stability of GR-TiO₂ over AO7 dye.

of the catalyst. Figure 9 shows the degradation mechanism of photocatalyst, where the photo-generated electrons transferred to excited state of conduction band (CB) from valance band (VB). Therefore, photo-generated holes are created on VB of TiO₂ spheres [25]. Subsequently, the photo-generated electrons will get transferred to graphene, which thoroughly contact on the surface of TiO₂ polycrystal spheres. Effective charge separation of photo-generated electrons and holes were maintained by graphene. Reactive oxygen species were formed by reaction of trapped electrons in graphene with the dissolved oxygen. Owing to this, decreased electron-hole recombination occurred. TiO₂ surface contains photo-generated electrons stucked directly by the dissolved oxygen to give reactive oxygen species, which react with water to give hydroxyl radicals, which is a strong oxidant towards degradation of AO7 [26–28]. A schematic illustration of the mechanism of improved photocatalytic efficiency of the GR–TiO₂ nanocomposites is shown in figure 9. The degradation mechanism was exposed as follows:

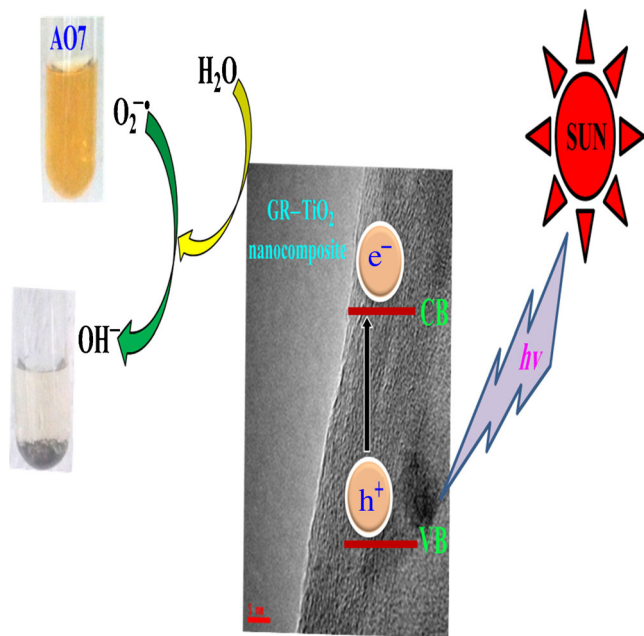
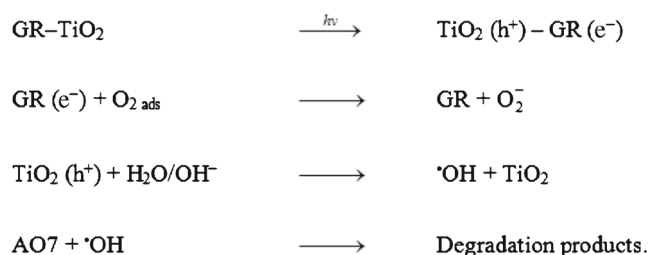


Figure 9. Photocatalytic degradation mechanism of catalyst with AO7 under solar light irradiation.

4. Conclusions

Fabrication of graphene–TiO₂ nanocomposite has been facile synthesized by a chemical process. The FESEM, TEM and HR-TEM show that the GR–TiO₂ nanoparticles were randomly anchored onto the graphene sheets. Photodegradation activity tests exposed that GR–TiO₂ material shows superior catalytic efficiency for AO7 dye compared to bare TiO₂, GR and mechanical mixture GR+TiO₂. This signifies that the electron transfer between GR and TiO₂ will greatly hinder the recombination of photo-induced charge carriers and extends the lifetime of electrons, which keeps in the improvement the lifetime of electrons of photocatalytic performance. GR–TiO₂ composites also show a superior stability due to the cycling tests. Therefore, solar light-sensitive catalyst facilities are used for environmental applications.

Acknowledgements

The present work was economically supported by University Grant Commission, New Delhi (Grant no. 2-362/2013 (SR)), and instrumental analysis supported by the University of Hyderabad, IIT Madras, Sri Venkateswara University, Tirupati and ICT Hyderabad is gratefully acknowledged. We are also thankful to Dr R V Jayanth Kasyap, Asst. Professor in English, Yogi Vemana University, Kadapa, India, for verifying the linguistic correctness.

References

- [1] Stankovich S, Dikin D A, Dommett G H B, Kohlhaas K M, Zimney E J, Stach E A *et al* 2006 *Nature* **442** 282
- [2] Geim A K and Novoselov K S 2007 *Nat. Mater.* **6** 183
- [3] Khalid N R, Ahmed E, Hong Z, Sana L and Ahmed M 2013 *Curr. Appl. Phys.* **13** 659
- [4] Lee J S, You K H and Park C B 2012 *Adv. Mater.* **24** 1084
- [5] Xiang Q, Yu J and Jaroniec M 2012 *Chem. Soc. Rev.* **41** 782
- [6] Xiang Q and Yu J 2013 *J. Phys. Chem. Lett.* **4** 753
- [7] Zhang N, Zhang Y H and Xu Y J 2012 *Nanoscale* **4** 5792
- [8] Yang M Q and Xu Y J 2013 *Phys. Chem. Chem. Phys.* **15** 19102
- [9] Yang M Q, Zhang N, Pagliaro M and Xu Y J 2014 *Chem. Soc. Rev.* **43** 8240
- [10] Habisreutinger S N, Schmidt-Mende L and Stolarczyk J K 2013 *Angew. Chem. Int. Ed.* **52** 2
- [11] Khan M M, Ansari S A, Pradhan D, Ansari M O, Han D H, Lee J *et al* 2014 *J. Mater. Chem. A* **2** 637
- [12] Novoselov K S, Geim A K, Morozov S V, Jiang D, Zhang Y, Dubonos S V, Grigorieva I V and Firsov A 2004 *Science* **306** 666
- [13] Kryukova G N, Zenkovetsa G A, Shutilova A A, Wilde M, Günther K, Fassler D *et al* 2007 *Appl. Catal. B Environ.* **71** 169
- [14] Zhang J, Wang P, Sun J and Jin Y 2014 *ACS Appl. Mater. Interf.* **6** 19905
- [15] Perreault F, Fonseca de Faria A and Elimelech M 2015 *Chem. Soc. Rev.* **44** 5861

- [16] Yuan L, Yu Q Q, Zhang Y H and Xu Y J 2014 *RSC Adv.* **4** 15264
- [17] Muthirulan P, Nirmala Devi C and Meenakshi Sundaram M 2014 *Ceram. Inter.* **40** 5945
- [18] Muthirulan P, Nirmala Devi C and Meenakshi Sundaram M 2014 *Adv. Mater. Lett.* **5** 163
- [19] Liang Y Y, Wang H L, Casalongue H N S C, Chen Z and Dai H J 2010 *Nano Res.* **3** 701
- [20] Hsieh S H, Chen W J and Wu C T 2015 *Appl. Surf. Sci.* **340** 9
- [21] Hummers W S and Offeman R E 1958 *J. Am. Chem. Soc.* **80** 1339
- [22] Lui G, Liao J Y, Duan A, Zhang Z, Fowler M and Yu A 2013 *J. Mater. Chem. A* **1** 12255
- [23] Akhavan O, Ghaderia E and Rahimi K 2012 *J. Mater. Chem.* **22** 23260
- [24] Kim J, Khoh W H, Wee B H and Hong J D 2015 *RSC Adv.* **5** 9904
- [25] Sun L, Zhao Z, Zhou Y and Liu L 2012 *Nanoscale* **4** 613
- [26] Gu L, Wang J, Cheng H, Zhao Y, Liu L and Han X 2013 *ACS Appl. Mater. Interf.* **5** 3085
- [27] Zhang H, Guo L H, Wang D, Zhao L and Wan B 2015 *ACS Appl. Mater. Interf.* **7** 1816
- [28] Venkata Ramana P, Viswadevarayalu A, Janardhan Reddy K, Varada Reddy A and Adinarayana Reddy S 2016 *Korean J. Chem. Eng.* **33** 456
- [29] Park C Y, Kefayat U, Vikram N, Ghosh T, Oh W C and Cho K Y 2013 *Bull. Mater. Sci.* **36** 869